Photoionization Dynamics of Ammonia (B^1E''): Dependence on Ionizing Photon Energy and Initial Vibrational Level†

Paul Hockett,‡ Michael Staniforth, and Katharine L. Reid*

School of Chemistry, University of Nottingham, Nottingham NG7 2RD, United Kingdom

Received: May 20, 2010; Revised Manuscript Received: July 28, 2010

In this article we present photoelectron spectra and angular distributions in which ion rotational states are resolved. This data enables the comparison of direct and threshold photoionization techniques. We also present angle-resolved photoelectron signals at different total energies, providing a method to scan the structure of the continuum in the near-threshold region. Finally, we have studied the influence of vibrational excitation on the photoionization dynamics.

1. Introduction

Molecular photoionization dynamics can be studied in exquisite detail when rotational state detection of the nascent cation can be achieved. This was demonstrated in pioneering work by Müller-Dethlefs and co-workers in the early days of the development of ZEKE (zero electron kinetic energy) spectroscopy,[1,2] and the current state-of-the-art attainable using ZEKE spectroscopy, or its sister technique MATI (mass analyzed threshold ionization) spectroscopy, is demonstrated by studies of ethylene and the allyl radical by Merkt and co-workers.[3,4] For the accurate determination of line positions, and hence spectroscopic constants, these techniques are unrivalled. However, additional insight into the dynamics of the photoionization process itself is provided by the use of complementary techniques. The reasons for this are that (a) the ZEKE experiment by its very nature is limited to the study of dynamics at the ionization threshold, (b) the observed intensities in a ZEKE spectrum are complicated by channel interactions[5] and experimental artifacts, and (c) rotational branching ratios alone do not always allow the relative phases of the photoelectron partial waves to be determined.[6,7] Ideally, the use of complementary techniques would enable these limitations to be assessed.

The capability of resolving cation rotational states is very rare in photoelectron spectroscopy, therefore there are few opportunities to assess the rotational branching ratios observed in ZEKE. Because of the continuity of oscillator strength across the ionization threshold, the results might be expected to be comparable with those from direct ionization experiments, with any differences observed pointing to the more complex ionization pathways available in the ZEKE case. De Lange and co-workers[8–10] were able to compare rotationally resolved ZEKE spectra with those obtained using a magnetic bottle photoelectron spectrometer for several diatomic molecules at high *J*, and observed significant differences in some cases. The case of HCl was most striking, with very different rotational and spin−orbit branching ratios observed using the two techniques. In the HCl example these differences were ascribed to the decay of ZEKE states via rotational or spin−orbit autoionization, highlighting the possibility of evolution of the initially populated Rydberg state population during the delay before field-ionization. As discussed by Chupka,[11] such behavior is generally to be expected, leading to rotational line strengths that are very different from those expected in direct photoionization. However, Chupka also points out that there are "various scenarios" in which rotational line intensities will be in "fairly good agreement with calculations"; indeed, orbital ionization model calculations[3] and multichannel quantum defect (MQDT) calculations[12] have been successful in matching ZEKE spectra. Because neither of these methods considers decay of ZEKE states prior to field ionization, their success provides some evidence that autoionization may, in many cases, only present a minor perturbation.

In recent work on the photoionization dynamics of NH_3 (B^1E'') we have shown that in some circumstances cation rotational resolution can be achieved using the technique of velocity map imaging (VMI) of photoelectrons,[13] and this has enabled us to obtain photoelectron angular distributions (PADs) associated with each rotational state.[7,14] In refs 7 and 14 we have analyzed in detail the photoionization dynamics out of the $v_2 = 4$ level in the B^1E'' state at a single photon energy; this analysis has enabled us to determine the radial dipole matrix elements that control the ionization process. Because the photoionization dynamics of the B^1E'' state have previously been studied using both ZEKE and MATI spectroscopy,[5,15,16] this system provides an ideal benchmark for comparison. In our experiments, as well as observing PADs we have also been able to tune the wavelength of the ionizing photon in order to investigate any energy dependence of the photoionization dynamics separately from the dependence on the cation state formed, and this previously unpublished data provides a focus for the discussion in the present work. In addition, we present new data on the photoionization dynamics out of the $v_2 = 3$ level in the B^1E'' state.

2. Experimental Section

Our experiments are carried out in a pump−probe ionization scheme in which photoelectron velocity map imaging (VMI) is employed. Details of the setup are given in ref 14; the only differences here concern changing the probe wavelength λ_{probe} as discussed below. To probe the energy dependence of the photoionization dynamics, two techniques were used. (1) Photoelectron images were recorded for incremental steps in λ_{probe}. (2) High-resolution continuous scans of λ_{probe}, which we

† Part of the "Klaus Müller-Dethlefs Festschrift".

‡ Present address: Steacie Institute for Molecular Sciences, National Research Council of Canada, 100 Sussex Drive, Ottawa, Ontario K1A 0R6 Canada.

10.1021/jp104623m
Published on Web 08/26/2010

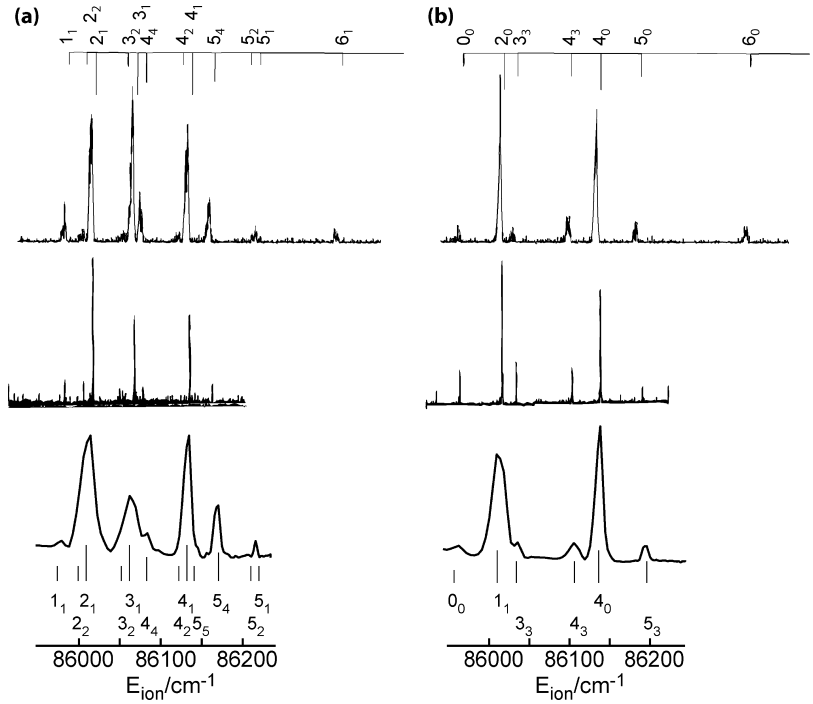

Figure 1. Comparison of MATI, ZEKE and VMI spectra. Top: MATI spectra, recorded via $\tilde{B}^1E''(v_2 = 2)$, adapted from ref 5. Middle: ZEKE spectra, recorded via $\tilde{B}^1E''(v_2 = 2)$, adapted from ref 16. Bottom: VMI spectra, recorded via $\tilde{B}^1E''(v_2 = 4)$. Panel (a) $J_K = 1_1 \rightarrow 3_2$, (b) $J_K = 1_0 \rightarrow 3_1$. The energy scale is correct only for the VMI data (see text). MATI and ZEKE spectra have been scaled to aid visual comparison. The rotational levels are labelled according to whether they are due to pπ Rydberg character (long lines), dδ Rydberg character (medium lines), or rescattering (short lines).

name "probe scans" in what follows, with real-time detection of both total and energy dispersed photoelectron yield, were recorded. These scans were obtained by gating over each rotational feature in the image, then tracking the features during the scan in order to maintain rotational selectivity for all λ_{probe}.

The benefit of the probe scan method is that it allows a high-resolution scan to be undertaken in a relatively short time: because there is no image inversion (and PADs are not obtained), the number of counts required per wavelength is greatly reduced from the norm. The disadvantage is that the peak intensities obtained directly from the uninverted images will be contaminated by intensities due to other features in the image. However, for well separated peaks, this contamination is likely to be minimal due to the geometric dispersion of the photoelectron velocity spheres over the image and will amount to only a slight, uniform, increase in the background contribution to the inner features. This method therefore provides a way to perform a survey scan over a large range of probe wavelengths in minimal time. Features observed in the scans can then be probed in detail by recording images at specific wavelengths of interest.

3. Results and Discussion

The $\tilde{B}^1E''$ electronic state of ammonia is an $n = 3$ Rydberg state in which the atoms adopt a planar geometry, and in the experiments described here it is prepared by a two-photon absorption step. The change in geometry on excitation generates favorable Franck-Condon factors for the formation of the $\tilde{B}^1E''$ state with relatively high quanta in ν_2, the "umbrella" vibrational mode. Strong parity, symmetry, and angular momentum selection rules control the rotational levels that can be prepared on excitation to, and ionization out of, the $\tilde{B}^1E''$ state.[17,18] The Rydberg series of which the $\tilde{B}^1E''$ state is a member converges on the $\tilde{X}^2A''_2$ ground state of the cation, therefore there is a strong propensity for the vibrational state to be unchanged on photoionization to the $\tilde{X}^2A''_2$ state; here we only consider these $\Delta v = 0$ transitions that are induced by one-photon ionization at varying wavelengths. In our previous work[14] we have discussed the propensities for forming the different cation rotational states by reference to the pπ/dδ orbital angular momentum character of the $\tilde{B}^1E''$ state. In brief, the most intense transitions are expected to originate directly from pπ, with minor transitions originating directly from dδ or as a result of photoelectron partial waves rescattering from the ion core.

3.1. Comparison with ZEKE/MATI Spectroscopy. Müller-Dethlefs and co-workers have recorded ZEKE spectra using the $v_2 = 2$ level in the $\tilde{B}^1E''$ state as the resonant intermediate,[16] whereas Softley and co-workers used the $v_2 = 2$, 4, and 6 levels as intermediates for their MATI spectra.[5] In our photoelectron VMI work we have used the $v_2 = 3$ and $v_2 = 4$ levels as intermediates. The rotational selection rules and rotational branching ratios are expected to be the same for $v_2 = 2$ and $v_2 = 4$, but different for $v_2 = 3$;[19] this has been verified in ref 5. Therefore, we are able to compare our $v_2 = 4$ data with the $v_2 = 2$ data obtained in the other studies; such a comparison is shown in Figure 1 for two different $\tilde{X}^2A''_2 \rightarrow \tilde{B}^1E''$ rotational transitions, $J_K = 1_1 \rightarrow 3_2$ and $1_0 \rightarrow 3_1$. The observed cation rotational levels have been assigned and are also labeled according to whether they result from pπ, dδ, or rescattering. Because of the difference in vibrational level, the MATI and ZEKE spectra are shifted relative to the VMI spectra, and the rotational level spacing will also be slightly different. In addition the 6_0 and 6_1 levels are observed in the MATI spectra; these were not energetically accessible in the imaging experiments with the probe wavelength used (431.52 nm), nor do they appear within the energy range shown in the ZEKE spectra of ref 16. For the $1_1 \rightarrow 3_2$ transition both the MATI and ZEKE spectra show evidence of features assigned to $K = 2$ in the ion, which

arise from $\Delta K = 0$ ionizing transitions. As expected,[5] these are weak features in the spectra and, although they are not resolved in the VMI spectra, do not make significant contributions to peak intensities. Once these factors are taken into account it can be seen that the rotational branching ratios obtained using the three techniques are in fact very different. For the $1_1 \rightarrow 3_2$ pump transition (Figure 1a) the most intense feature in the MATI spectrum, assigned to $J_K = 3_1$, is the least intense pπ allowed feature in the equivalent ZEKE and VMI spectra. Further, whereas the 2_1 and 4_1 features are of similar intensities in the VMI and MATI spectra, they have very different intensities in the ZEKE spectrum, and the 5_4 feature is much less intense in the ZEKE spectrum than in either the VMI or MATI data. The spectra recorded via the $1_0 \rightarrow 3_1$ pump transition (Figure 1b) show fewer differences, but notable among them are significant changes in the relative intensities of the pπ allowed features; the 0_0 scattering feature is also considerably more intense in the ZEKE spectrum.

There are many factors that can influence the intensities seen in the ZEKE experiments, some of which are controlled by the experimental conditions and some of which result from inherent molecular properties. In particular, the observed signal is very sensitive to any stray electric fields present, and small changes can lead to significant changes in l and m_l mixing of the high-n Rydberg states. This mixing creates the so-called ZEKE states that contribute to the pulsed field ionization step in both ZEKE and MATI spectroscopy.[20,21] Differences in the stray fields could be caused simply by the degree of electrical shielding in the experiments, but more subtly the electric fields present will also be affected by the number of ions created in the experiment[20,22] and therefore the gas density, laser power, and focal volume may all produce changes in the observed signal by affecting the character and hence the lifetime of the ZEKE states populated. Differences in the observed intensities between ZEKE studies are therefore not surprising as the experimental conditions will be different.

In situations where decay channels are available to the ZEKE states differences between ZEKE and direct photoionization are also to be expected. If the ZEKE states are short-lived then changes in the branching ratios between the ZEKE and direct ionization pathways may be significant. This was exactly the case observed by De Lange and co-workers in HCl,[8] and ascribed to autoionizing ZEKE states as discussed above. Channel interactions between Rydberg manifolds converging on different ion rotational levels have also been observed in ZEKE.[23,24] Such interactions have been classed as "pseudo autoionization" and can create substructure in ZEKE spectra.[5,19]

Despite the issues raised above, the fact that the same rotational levels are populated in the VMI and ZEKE/MATI data suggests that the ionization dynamics are broadly similar in both cases. This implies that there are not significant perturbations to the spectra from autoionizing channels accessible to the high-n ZEKE states created prior to field ionization in the ZEKE/MATI results. However, the differences in branching ratios observed in the ZEKE and MATI experiments underscores the difficulty of using these observables alone in order to determine photoionization dynamics. Photoelectron angular distributions inherently provide additional insight into photoionization dynamics, and our experiments provide a means of independently determining branching ratios. These considerations highlight the complementary nature of these techniques.

3.2. Probe Wavelength Dependence.

3.2.1. Observations. In our previous work we have used our measured rotationally resolved photoelectron angular distributions to deduce photoionization dynamics[7,14] from our experiments. In order to make this deduction the assumption that there is no photoelectron kinetic energy dependence over the range studied ($\sim$200 cm^{-1} for the $v_2 = 4$ data set presented in refs 7 and 14) was made. The validity of this assumption is then verified by the good agreement between the spectra and PADs calculated using the determined dynamical parameter set, and those measured in the experiment. Although this assumption generally holds well, a few discrepancies between the calculated and experimental results suggest that in some instances the underlying physics is not captured in the set of dynamical parameters that model the remaining data convincingly. The most notable discrepancy is seen in the PAD associated with the 1_1 ion rotational state that clearly differs from the prediction;[14] data from ref 14 is also reproduced in Figure 10 in this work.

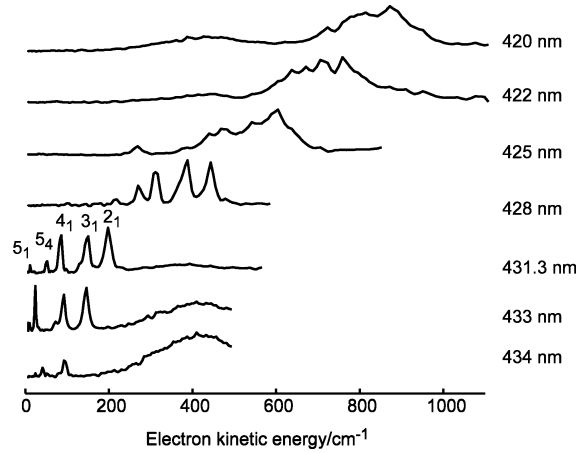

Figure 2. Dynamic range dependence of photoelectron image resolution. Spectra are labeled by ionizing wavelength, λ_{probe}. For λ_{probe} = 431.3 nm rotational features are also labeled.

In the work presented here we have investigated this behavior further by varying the probe laser wavelength, λ_{probe}, in order to study the rotational branching ratios and PADs as a function of electron kinetic energy for any given feature in the spectrum. Because of the need to preserve rotational resolution, we are limited to a small energy window in the near threshold region. This is illustrated in Figure 2, where we show that probe wavelengths shorter than $\sim$428 nm lead to a loss of rotationally resolved features. Nevertheless, using this technique we have a good compromise between ZEKE (rotational resolution at a single electron kinetic energy) and traditional photoelectron spectroscopy (poor resolution at a wide range of electron kinetic energies), enabling new insight into ionization dynamics through a detailed mapping of the near-threshold region of the ionization continuum.

The two methods used to probe energy dependence were described in the Experimental Section. For these studies we concentrated on the ion rotational states formed following excitation through the intense $\tilde{X}^1A''_1(v = 0, 1_1) \rightarrow \tilde{B}^1E''(v_2 = 4,3_2)$ pump transition. The previously published ion rotational branching ratios have already been shown in Figure 1a, where it can be seen that the most intense lines are assigned to the 2_1 and 4_1 ion rotational states, with significant contributions from 3_1, 5_1, and 5_4. The transition to the 1_1 ion state makes only a very small contribution at this probe wavelength (431.52 nm). After initial scans of the probe wavelength, a selection of images were recorded; integrated peak intensities obtained from these images after processing are shown in Figure 3 along with results from the probe wavelength scan. Both sets of traces show clear

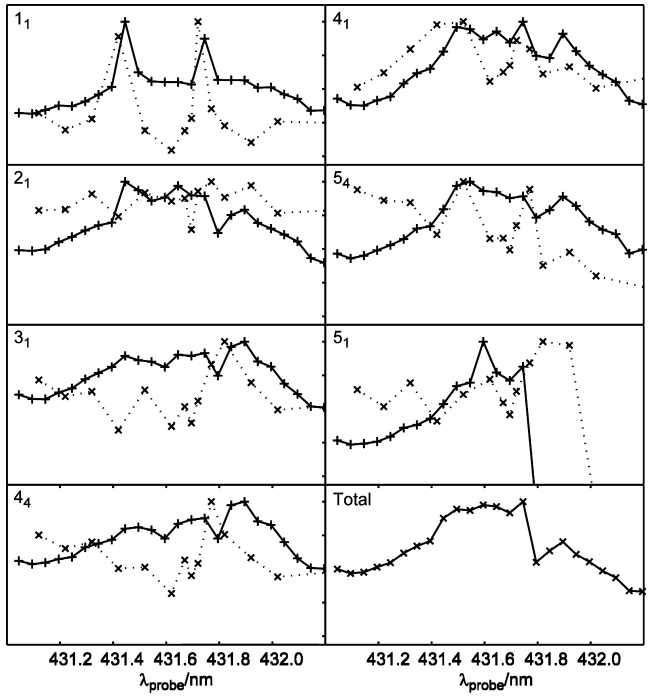

Figure 3. Probe wavelength scans (solid line) and integrated peak intensities obtained from processed images (dotted line). Each panel correlates to a different ion rotational state as labeled; shown in the "total" panel is the integrated probe scan data. The plot for each channel is set to a zero to unity scale to aid comparison.

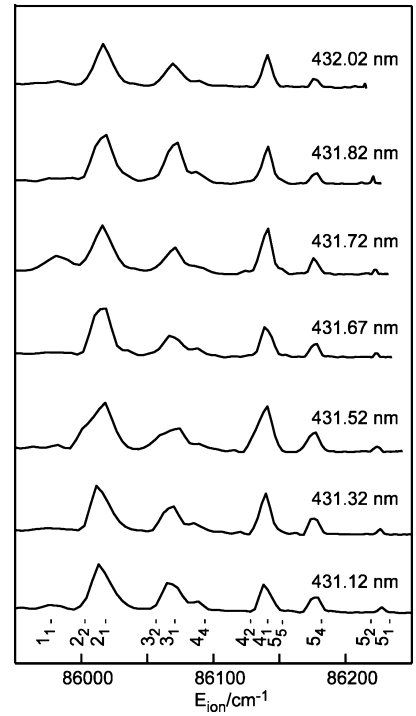

Figure 4. Photoelectron spectra as a function of ionizing wavelength, λ_{probe}. Spectra were extracted from inverted photoelectron images. Changes in peak intensities visible in the spectra can be compared with the peak intensity data shown in Figure 3.

changes in peak intensities as a function of λ_{probe}, although there are some differences between the traces obtained directly from the probe scan versus those obtained from processed images. The clearest change is seen in the 1_1 channel. The intensity of this feature as a function of probe wavelength shows two sharp peaks at $\lambda_{probe} = 431.42$ and 431.67 nm. The 5_4 channel shows similar features at 431.52 and 431.77 nm, that is, shifted by 0.1 nm relative to the peaks in the 1_1 channel, although these features are not so apparent in the probe scan result. Changes in the other channels appear more oscillatory in nature, with no clear patterns. The sharp cutoff in the 5_1 channel occurs when there is no longer enough probe energy to access this state in the ion; the apparent difference between this cutoff in the probe versus image data is due to the width of the gating in the probe scan case. In Figure 4 we show the full photoelectron spectrum obtained from the images obtained at selected probe wavelengths. In this form the changes in the 3_1 and 4_1 channels are very clear and appear as oscillations in the peak heights. For example, at 431.12 nm the 3_1 and 4_1 peaks are roughly equal in intensity, at 431.52 nm the 4_1 feature is more intense, and at 431.82 nm the peak intensities are again similar.

From these images, PADs can also be obtained that correspond to each ion rotational state, and significant changes are also seen in these results. In the situation where the two-photon excitation step and one-photon ionization step are effected with light that is linearly polarized along the same lab frame axis the angle resolved photoelectron intensity, $I(\theta,\phi)$, can be expressed by:

$$I(\theta,\varphi) = \beta_{00}\{1 + \beta_{20}Y_{20}(\theta,0) + \beta_{40}Y_{40}(\theta,0) + \beta_{60}Y_{60}(\theta,0)\}$$

We show in Figure 5 the behavior of the anisotropy parameters, β_{L0} plotted as a function of probe wavelength, and explicitly plot the PADs for just two channels in Figure 6. In general, all the β_{L0} for any given channel change as a function of probe wavelength, with the most significant changes seen in β_{20}. In some cases, for example the 3_1 channel, the PAD is almost invariant to probe wavelength; in other cases, for instance the 4_1 channel, the PAD changes significantly with probe wavelength. The changes in the PADs do not appear to match changes in the peak intensities in the rotational spectra, with the exception of the 1_1 feature. This may, however, be misleading as the β_{LM} extracted for cases where the feature is weak may be unreliable. There also appears to be little correlation between the changes observed in different channels. In short, the response of the spectra and PADs to the probe wavelength appears complex with no patterns immediately apparent. However, from Figure 5 it is apparent that the data analyzed in our previous work[7,14] recorded at 431.52 nm, lies in a relatively flat region of the continuum. The most rapid changes in the β_{L0} for all ion rotational states except 4_4, appear for $\lambda_{probe} > 431.60$ nm, although there are small changes in the β_{L0} (as well as changes in the peak intensities as discussed above) over the whole range probed.

3.2.2. Discussion. Work is ongoing to ascertain the causes of the behavior observed here, but we offer some general discussion toward a solution. The changes observed in both branching ratios and PADs indicate changes in the ionization dynamics, that is, the partial cross sections and/or phases, as a function of λ_{probe}. Because we have been able to determine a set of dynamical parameters that fit the data at a single probe wavelength and therefore are consistent over a range of photoelectron kinetic energies ($\sim$200 cm^{-1}); it seems that the changes with probe wavelength must reflect structure in the continuum. If this structure is discrete, then at some values of λ_{probe} we might, by chance, observe mostly the underlying dynamics whereas, at other wavelengths and/or in a specific channel, we observe the effects of this continuum structure.

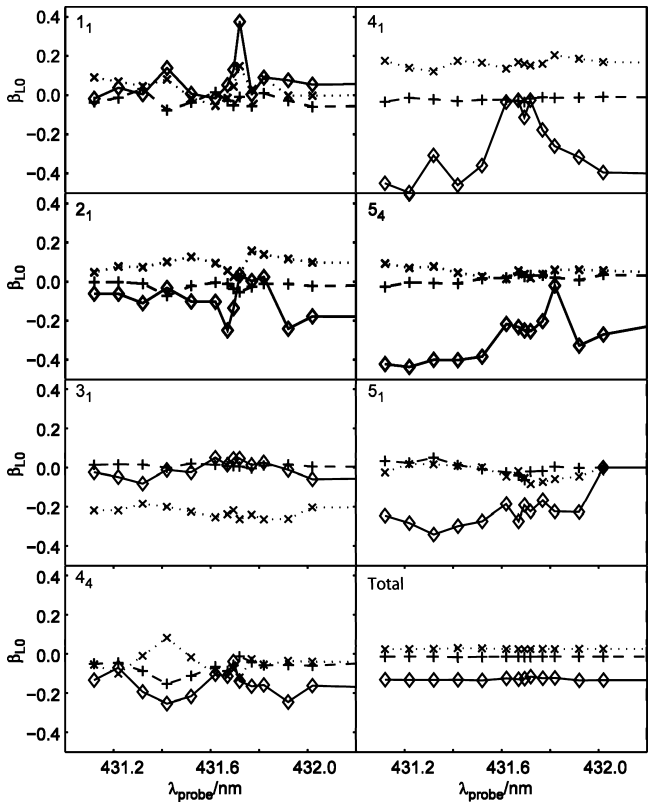

Figure 5. Normalized anisotropy parameters, β_{L0}, as a function of ionizing wavelength, λ_{probe}. Plots show parameters for $L = 2$ (solid line, diamond markers), $L = 4$ (dotted line, $\times$ markers) and $L = 6$ (dashed line, $+$ markers). The parameters were obtained from each feature in the photoelectron images and are labeled by ion rotational level. Anisotropy parameters obtained from summing the data over all ion rotational levels are shown in the final panel.

Rotationally summing the PADs reduces the data to a single set of β_{LM} that appear invariant to λ_{probe}; see Figure 5. This behavior is consistent with changes in only a few of the partial waves, effects which are washed out by rotational summation. In a case where the underlying dynamics shifted significantly over the range studied, changes may be expected in the rotationally summed data.

By changing λ_{probe} the total ionization energy is shifted, as is the photoelectron kinetic energy correlated with the formation of any given ion rotational state. Our measurements could therefore be sensitive to:

(a) Channel interactions between discrete[25,26] and continuum states. The effect of such channel coupling on PADs from atomic systems has previously been observed, see for example refs 27 and 28, and shows some similarities to the phenomena observed in this work. PADs correlated with autoionizing levels in the photoionization of diatomic systems have also been observed, see for example refs 29 and 30. Although vibrational autoionization in ammonia is well-known,[31] the small probe wavelength range studied in this work is suggestive of rotational autoionization. However, the highly restrictive selection rules for this process[32] make it hard to find likely candidates.

(b) Changes in the scattering dynamics as a function of photoelectron kinetic energy. Shifts in the relative phases of certain partial waves could provide an explanation for the complicated patterns shown in the data, while still allowing for a consistent set of dynamical parameters to be found in flat regions of the continuum.

As discussed above, and in our previous work,[7,14] the success of our analysis in fitting the observed PADs for different

Figure 6. Photoelectron angular distributions for (a) the 3_1 channel and (b) the 4_1 channel recorded with selected ionizing wavelengths, λ_{probe}. PADs are plotted in polar form using the anisotropy parameters shown in Figure 5, which were obtained from inverted photoelectron images. For clarity, error bars are not shown, but in all cases are small and of comparable magnitude to those shown in Figure 10(a).

vibrational levels and polarization geometries validates the assumption of a flat continuum. The data presented here show that, even in this apparently favorable case, the near-threshold region of the continuum is very complex. Further work is required to ascertain the full nature and extent of this behavior.

3.3. Results Obtained Following Ionization from $v_2 = 3$. In our previously published work, and in the previous section, we considered $\Delta v = 0$ ionizing transitions to the electronic ground state of the ion, $\tilde{X}^1A''_1(v_2 = 4, J_K)$, via several rovibronic pump transitions of the form $\tilde{X}^1A''_1(v = 0, J_K) \rightarrow \tilde{B}^1E''(v_2 = 4, J_K)$. In order to probe the vibrational dependence of the ionization dynamics data was also recorded via $\tilde{B}^1E''(v_2 = 3, J_K)$. Because of the rovibrational selection rules[18] it is not possible to access the same set of transitions used in the $v_2 = 4$ case, however, the $1_1 \rightarrow 2_2$ and $1_1 \rightarrow 3_2$ pump transitions are allowed in both cases, and the resulting photoelectron spectra and PADs can be compared. As shown in our previous publications,[7,14] we were able to determine the set of partial wave cross sections and phase shifts characterizing the ionization for the $v_2 = 4$ case. Using these parameters we can calculate rotational spectra for any given ionizing transition; such calculated spectra therefore also provide a means to test whether the ionization dynamics change considerably between $v_2 = 3$ and $v_2 = 4$.

In Figure 7 we show the spectra obtained via $\tilde{B}^1E''(v_2 = 3, J_K)$, along with the spectra calculated using the dynamical parameters obtained for the $v_2 = 4$ case.[14] In most cases good

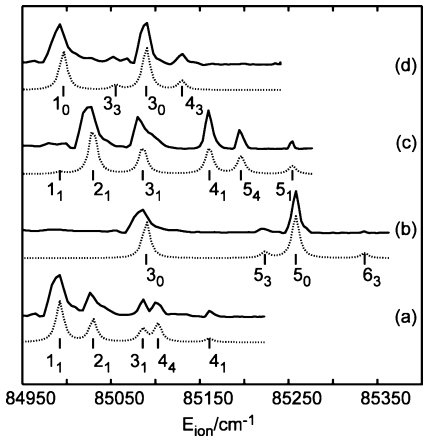

Figure 7. Photoelectron spectra for the four $\tilde{X}^1A''_1(v = 0, J_K) \rightarrow \tilde{B}^1E''(v_2 = 3, J_K)$ transitions studied; (a) $1_1 \rightarrow 2_2$, (b) $2_0 \rightarrow 4_1$, (c) $1_1 \rightarrow 3_2$, (d) $0_0 \rightarrow 2_1$. Ion rotational levels are labelled by J_K. Calculated spectra, using the dynamical parameters determined from the $\tilde{X}^1A''_1(v = 0, J_K) \rightarrow \tilde{B}^1E''(v_2 = 4, J_K)$ data set, are also shown for comparison (dashed lines).

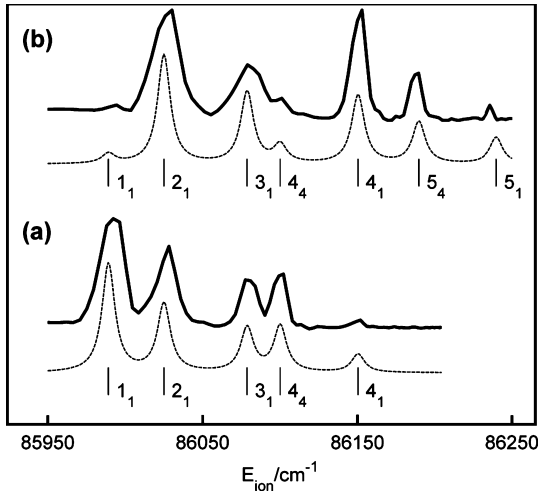

Figure 8. Photoelectron spectra for two of the six $\tilde{X}^1A''_1(v = 0, J_K) \rightarrow \tilde{B}^1E''(v_2 = 4, J_K)$ transitions studied;[14] (a) $1_1 \rightarrow 2_2$, (b) $1_1 \rightarrow 3_2$. These can be compared to spectra a and c in Figure 7. Ion rotational levels are labeled J_K. Calculated spectra are also shown for comparison (dashed lines).

agreement is observed between the experimental and calculated spectra, suggesting that there is little change in the dynamical parameters governing the ionziation between the two cases. In Figure 8 we show the two directly comparable spectra recorded via $\tilde{B}^1E''(v_2 = 4, J_K)$. Again there is generally good agreement between the spectra and calculations, and the $v_2 = 3$ results. There are some exceptions, in particular the 4_1 feature for the spectra recorded via $1_1 \rightarrow 3_2$ for both $v_2 = 3$ and 4 (Figure 7c and Figure 8b, respectively) is more intense than predicted by the calculation. For the $v_2 = 3$ case the branching ratio of the 3_0 and 5_0 peak recorded via $2_0 \rightarrow 4_1$ (Figure 7b) is also not reproduced in the calculation, although this apparent discrepancy may partly be due to the differing peak widths in the experimental spectra, which occurs due to the nonlinear conversion from velocity to energy. However, overall the spectra and calculations suggest that there is no significant difference in the ionization dynamics between $v_2 = 3$ and 4. A similar conclusion was reached in the MATI work of Dickinson et al.,[5] in which spectra recorded via $\tilde{B}^1E''(v_2 = 2, J_K)$, $\tilde{B}^1E''(v_2 = 4, J_K)$ and $\tilde{B}^1E''(v_2 = 6, J_K)$ were compared, and little or no change was observed in the rotational branching ratios in all cases.

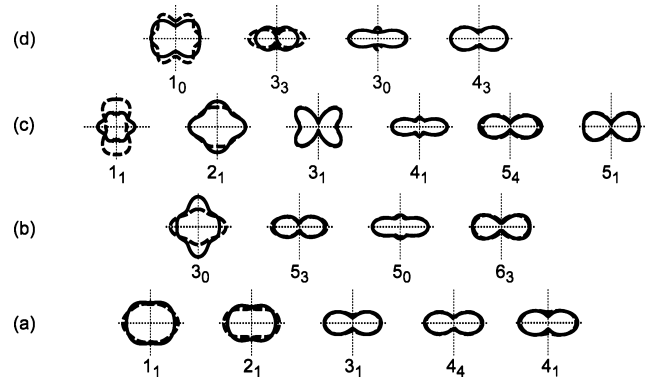

Figure 9. Photoelectron angular distributions for the four $\tilde{X}^1A''_1(v = 0, J_K) \rightarrow \tilde{B}^1E''(v_2 = 3, J_K)$ transitions studied; (a) $1_1 \rightarrow 2_2$, (b) $2_0 \rightarrow 4_1$, (c) $1_1 \rightarrow 3_2$, (d) $0_0 \rightarrow 2_1$. PADs are plotted in polar coordinates. Ion rotational levels are labelled by J_K. Calculated PADs, using the dynamical parameters determined from the $\tilde{X}^1A''_1(v = 0, J_K) \rightarrow \tilde{B}^1E''(v_2 = 4, J_K)$ data set, are also shown for comparison (dashed lines).

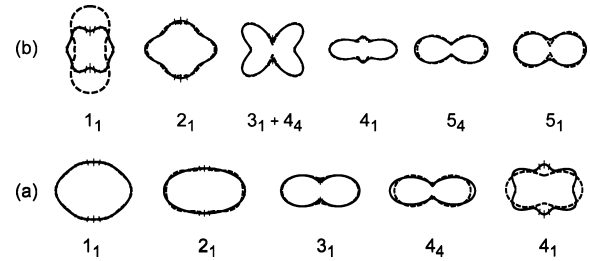

Figure 10. Photoelectron angular distributions for two of the six $\tilde{X}^1A''_1(v = 0, J_K) \rightarrow \tilde{B}^1E''(v_2 = 4, J_K)$ transitions studied;[14] (a) $1_1 \rightarrow 2_2$, (b) $1_1 \rightarrow 3_2$. These can be compared to panels (a) and (c) in Figure 9. Ion rotational levels are labeled J_K. Calculated PADs are also shown for comparison (dashed lines).

As previously discussed, our VMI measurements also provide the photoelectron angular distributions, which are very sensitive to the ionization dynamics via the partial wave phases. In fact, as shown in previous work,[6,7,14,33] it is this sensitivity that allows us to deduce the dynamical parameters from our experimental results, even when there are many partial waves involved. The same calculations that allow us to predict the rotational spectra also allow us to calculate the PADs for any given ionizing transition.[14] We can therefore again make use of the dynamical parameters obtained for the $v_2 = 4$ case as a means to check for changes in the ionization dynamics as a function of vibrational excitation.

In Figure 9 we show both the experimental and calculated PADs for the $v_2 = 3$ data set. As was the case for the rotational spectra good agreement is seen in most cases, with a couple of notable exceptions. In particular the PADs correlated with the formation of $\tilde{X}^1A''_1(v_2 = 3, 1_0)$ (Figure 9d), $\tilde{X}^1A''_1(v_2 = 3, 1_1)$ (Figure 9c) and $\tilde{X}^1A''_1(v_2 = 3, 3_0)$ (Figure 9b) do not show as close agreement with the experimental data as the other calculated PADs. In Figure 10, which is analogous to Figure 8, we show the two pump transitions for the $v_2 = 4$ case that are directly comparable. Again, the PAD correlated with formation of $\tilde{X}^1A''_1(v_2 = 4, 1_1)$ via the $1_1 \rightarrow 3_2$ pump transition (Figure 10b) is not well-matched by the calculation. The same is true of the PAD correlated with formation of $\tilde{X}^1A''_1(v_2 = 4, 4_1)$ shown in Figure 10a. In the $v_2 = 4$ case, both of the PADs which do not match well to the calculated PADs were extracted from weak features in the data, so they may be somewhat unreliable. The fact that the 4_1 PAD shown in Figure 9a matches well to the calculated distribution for the $v_2 = 3$ case, and the corresponding peak in the spectrum is intense, corroborate this

supposition. However, the 3_0 PAD in the $v_2 = 3$ case (Figure 9b) is extracted from a strong spectral feature but does not agree with the calculated PAD. In this case the PAD is reliable, so this discrepancy must be meaningful.

As we discussed with regard to the probe wavelength dependence (Section 3.2), disagreement between experimental and calculated PADs in specific ionization channels may indicate subtle changes in the ionization dynamics that do not impinge on the whole set of observed PADs, or on the rotational spectra. Such behavior could be possible, for instance, if there were a small change in one of the partial wave amplitudes or phases either as a function of vibrational excitation or photoelectron kinetic energy. Because different ionization channels respond differently to any given partial wave, as a consequence of the complicated angular momentum coupling involved,[14] certain channels will be more sensitive to certain dynamical parameters. If the change is due to a genuine difference in dynamics between photoionization from $v_2 = 3$ and photoionization from $v_2 = 4$ then we might expect to see worse agreement with the calculated spectra and PADs over the whole data set. If, on the other hand, the difference occurs as a function of photoelectron kinetic energy over a small region of the spectrum, then it could be the case that certain channels have ionization dynamics that are significantly different from the norm; possible mechanisms for such continuum structure have been discussed in the previous section.

In summary, it seems that, with one or two exceptions, the ionization dynamics is essentially unchanged between $v_2 = 3$ and $v_2 = 4$. Physically, we can rationalize this on the basis that the small change in vibrational motion between the two cases should not significantly affect the scattering potential experienced by the outgoing photoelectron. This picture is strengthened by the fact that the $\bar{B}^1E''$ state is a low-lying Rydberg state, so we might expect that the Rydberg electron that is subsequently photoionized to be only weakly coupled to the nascent ion core. This implies that the bound state and the scattering state are relatively insensitive to the exact molecular geometry and, hence, vibrational excitation. This picture is likely to break down in the presence of large amplitude vibrational motion, or for cases where the state prepared prior to ionization is not of Rydberg character. Finally, we note the interesting possibility in this case of probing the strength of interaction of the Rydberg electron with the ion core by means of ionizing via different *n* Rydberg levels.

4. Conclusions

In this article we have presented photoelectron spectra and angular distributions in which ion rotational states are resolved. This data enables the comparison of direct and threshold photoionization techniques. Such comparisons are rare because of the difficulty of obtaining rotational resolution in photoelectron spectroscopy, but are essential for examining fundamental differences in the processes that occur in each case. Although our measurements show similarities in the underlying photoionization dynamics, significant differences are observed in the rotational branching ratios obtained.

We have used the probe scan technique with rotational state selectivity to provide a survey scan over a range of probe wavelengths, and also measured angle-resolved photoelectron signal at different total energies. These methods provide a means to scan the structure of the continuum in the near-threshold region. Although the results of the probe scan experiments do not agree precisely with the imaging results, they provide a useful means of ascertaining the existence of continuum structure before more detailed (and time-consuming) measurements are undertaken. We have proposed mechanisms to explain the observed behavior, but insufficient information is available for a full interpretation. Although it is clear that more attention should be paid to the near-threshold energy dependence of photoionization dynamics, we note that in this instance it has nonetheless been possible to completely determine the dynamical parameters controlling the underlying direct photoionization process.[14]

Finally, we have considered the effect of vibrational excitation on the photoionization dynamics. As expected for ionization of an excited state of Rydberg nature, coupling to the nascent ion core is observed to be weak, and the photoionization dynamics virtually insensitive to vibrational excitation.

Acknowledgment. P. H. thanks H. J. Wörner for helpful discussions. Funding for this work was provided by the EPSRC through grant EP/C50013X.

References and Notes

(1) Mullerdethlefs, K.; Sander, M.; Schlag, E. W. *Z. Naturfors., A: Phys. Sci.* **1984**, *39*, 1089.
(2) Habenicht, W.; Baumann, R.; Mullerdethlefs, K.; Schlag, E. W. *Ber. Bunsen-Ges. Phys. Chem. Chem. Phys.* **1988**, *92*, 414.
(3) Willitsch, S.; Merkt, F. *Int. J. Mass Spectrom.* **2005**, *245*, 14.
(4) Gasser, M.; Schulenburg, A. M.; Dietiker, P. M.; Bach, A.; Merkt, F.; Chen, P. *J. Chem. Phys.* **2009**, *131*, 8.
(5) Dickinson, H.; Rolland, D.; Softley, T. P. *J. Phys. Chem. A* **2001**, *105*, 5590.
(6) Leahy, D. J.; Reid, K. L.; Zare, R. N. *J. Chem. Phys.* **1991**, *95*, 1757.
(7) Hockett, P.; Staniforth, M.; Reid, K. L.; Townsend, D. *Phys. Rev. Lett.* **2009**, *102*, 253002.
(8) De Beer, E.; Buma, W. J.; Delange, C. A. *J. Chem. Phys.* **1993**, *99*, 3252.
(9) Milan, J. B.; Buma, W. J.; deLange, C. A. *J. Chem. Phys.* **1996**, *104*, 521.
(10) Wales, N. P. L.; Buma, W. J.; deLange, C. A.; LefebvreBrion, H.; Wang, K. S.; McKoy, V. *J. Chem. Phys.* **1996**, *104*, 4911.
(11) Chupka, W. A. *J. Chem. Phys.* **1993**, *98*, 4520.
(12) Softley, T. P.; Hudson, A. J. *J. Chem. Phys.* **1994**, *101*, 923.
(13) Eppink, A. T. J. B.; Parker, D. H. *Rev. Sci. Instrum.* **1997**, *68*, 3477.
(14) Hockett, P.; Staniforth, M.; Reid, K. L. *Mol. Phys.* **2010**, *108*, 1045.
(15) Seiler, R.; Hollenstein, U.; Softley, T. P.; Merkt, F. *J. Chem. Phys.* **2003**, *118*, 10024.
(16) Habenicht, W.; Reiser, G.; Mueller Dethlefs, K. *J. Chem. Phys.* **1991**, *95*, 4809.
(17) Ashfold, M. N. R.; Dixon, R. N.; Stickland, R. J.; Western, C. M. *Chem. Phys. Lett.* **1987**, *138*, 201.
(18) Signorell, R.; Merkt, F. *Mol. Phys.* **1997**, *92*, 793.
(19) Dickinson, H.; Rolland, D.; Softley, T. P. *Philos. Trans. R. Soc., A* **1997**, *355*, 1585.
(20) Softley, T. P.; Rednall, R. J. *J. Chem. Phys.* **2000**, *112*, 7992.
(21) Cockett, M. C. R. *Chem. Soc. Rev.* **2005**, *34*, 935.
(22) Procter, S. R.; Webb, M. J.; Softley, T. P. *Faraday Discuss.* **2000**, *115*, 277.
(23) Merkt, F.; Softley, T. P. *Int. Rev. Phys. Chem.* **1993**, *12*, 205.
(24) Softley, T. P. *Int. Rev. Phys. Chem.* **2004**, *23*, 1.
(25) Fano, U. *Phys. Rev.* **1961**, *124*, 1866.
(26) Fano, U.; Cooper, J. W. *Phys. Rev.* **1965**, *137*, 1364.
(27) Tauro, S.; Liu, K. P. *J. Phys. B* **2008**, *41*, 225001.
(28) Samson, J. A. R.; Gardner, J. L. *Phys. Rev. Lett.* **1973**, *31*, 1327.
(29) Mank, A.; Drescher, M.; Huthfehre, T.; Schonhense, G.; Bowering, N.; Heinzmann, U. *J. Phys. B* **1989**, *22*, L487.
(30) Park, H.; Konen, I.; Zare, R. N. *Phys. Rev. Lett.* **2000**, *84*, 3819.
(31) Raptis, C. A.; Pratt, S. T. *J. Chem. Phys.* **2001**, *115*, 2483.
(32) Raptis, C. A.; Pratt, S. T. *Chem. Phys. Lett.* **1999**, *303*, 281.
(33) Hockett, P.; Reid, K. L. *J. Chem. Phys.* **2007**, *127*, 154308.

JP104623M